2015

Investigation of Plasmon Resonance Tunneling through Subwavelength Hole Arrays in Highly Doped Conductive ZnO Films

Nima Nader

Shivashankar Vangala

Joseph R. Hendrickson

Kevin D. Leedy

David C. Look
Wright State University - Main Campus, david.look@wright.edu

See next page for additional authors

AIP | Journal of Applied Physics

Investigation of plasmon resonance tunneling through subwavelength hole arrays in highly doped conductive ZnO films

Nima Nader, Shivashankar Vangala, Joshua R. Hendrickson, Kevin D. Leedy, David C. Look, Junpeng Guo, and Justin W. Cleary

Citation: Journal of Applied Physics **118**, 173106 (2015); doi: 10.1063/1.4934875
View online: http://dx.doi.org/10.1063/1.4934875
View Table of Contents: http://scitation.aip.org/content/aip/journal/jap/118/17?ver=pdfcov
Published by the AIP Publishing

Investigation of plasmon resonance tunneling through subwavelength hole arrays in highly doped conductive ZnO films

Nima Nader,[1,2,a)] Shivashankar Vangala,[1,2] Joshua R. Hendrickson,[2] Kevin D. Leedy,[2] David C. Look,[2,3,4] Junpeng Guo,[5] and Justin W. Cleary[2]
[1]*Solid State Scientific Corporation, 12 Simon St., Nashua, New Hampshire 03060, USA*
[2]*Air Force Research Laboratory, Sensors Directorate, 2241 Avionics Circle, Wright Patterson AFB, Ohio 45433, USA*
[3]*Wyle Laboratories, Inc., 2601 Mission Point Blvd., Suite 300, Dayton, Ohio 45435, USA*
[4]*Semiconductor Research Center, Wright State University, Dayton, Ohio 45435, USA*
[5]*Department of Electrical and Computer Engineering, University of Alabama in Huntsville, 301 Sparkman Drive, Huntsville, Alabama 35899, USA*

(Received 4 June 2015; accepted 18 October 2015; published online 6 November 2015)

Experimental results pertaining to plasmon resonance tunneling through a highly conductive zinc oxide (ZnO) layer with subwavelength hole-arrays is investigated in the mid-infrared regime. Gallium-doped ZnO layers are pulsed-laser deposited on a silicon wafer. The ZnO has metallic optical properties with a bulk plasma frequency of 214 THz, which is equivalent to a free space wavelength of 1.4 μm. Hole arrays with different periods and hole shapes are fabricated via a standard photolithography process. Resonant mode tunneling characteristics are experimentally studied for different incident angles and compared with surface plasmon theoretical calculations and finite-difference time-domain simulations. Transmission peaks, higher than the baseline predicted by diffraction theory, are observed in each of the samples at wavelengths that correspond to the excitation of surface plasmon modes.
[http://dx.doi.org/10.1063/1.4934875]

I. INTRODUCTION

Plasmon resonance tunneling is a phenomenon in which transmission through sub-wavelength periodic apertures is larger than what was predicted by classical aperture theory.[1,2] This phenomenon is also called "extraordinary optical transmission," which has been well-investigated over the past decade.[3–5] Recent works have studied mid-infrared (mid-IR) surface plasmon polaritons (SPPs) on dysprosium-doped CaO[6] and arrayed structures fabricated in doped-Si,[7] InAs,[8] GaAs,[9,10] and InSb[11] as well as Cu-coated[12] and Ni[5,13] meshed structures with the doped-GaAs and Cu/Ni systems being specifically investigated.

The investigation of alternative plasmonic materials has recently been accelerated[7,14–26] due to the push to the infrared where noble metals are not as useful due to weak mode confinement and lack of CMOS compatibility. Two promising candidates, aluminum and gallium doped ZnO, have been proposed as possible plasmonic materials in the near-[17,19] and mid-IR[26] as these materials typically demonstrate plasma wavelengths $\sim$1 μm. ZnO also has displayed largely varying free carrier concentration and mobility[27–29] with slight changes in fabrication techniques and stoichiometry. These material properties are ultimately responsible in determining SPP properties such as propagation length and penetration depth,[26] which are important in waveguide and plasmonic circuit applications. Recent work has demonstrated the possibilities for ZnO based hybrid plasmonic-photonic waveguides.[30,31] Due to these features and its CMOS compatibility, we utilize doped ZnO as our infrared plasmonic material.

Recent investigations have demonstrated SPP coupling on highly conductive ZnO via hole arrays.[15,32] Presented in this paper are experimental results along with analytical and numerical calculations pertaining to surface plasmon resonance enhanced optical transmission of $\sim$1 μm deep ZnO hole arrays on a silicon substrate. Fig. 1 shows a schematic of the device structure investigated in this paper.

II. THEORETICAL AND EXPERIMENTAL DETAILS

The SPP wavevector is needed for analytical calculations of SPP excitations, and can be found according to Ref. 33

$$k_{spp} = \frac{2\pi}{\lambda}\mathrm{Re}\left[\sqrt{\frac{\varepsilon_d\varepsilon_c(\lambda)}{\varepsilon_d+\varepsilon_c(\lambda)}}\right], \quad (1)$$

where ε_d and ε_c are the permittivities of the dielectric and conductor, respectively, with the latter taken to be complex. Excitation of SPPs requires a coupling mechanism to compensate for the momentum mismatch between the free-space radiation and the SPP wavevector. Periodic structures, such as lamellar gratings or hole arrays, can provide such coupling due to an additional $2\pi/P$ momentum component where P is the modulation period. The photonic to plasmonic coupling condition then reads[5]

a)Author to whom correspondence should be addressed. Electronic mail: nima.nader@nist.gov

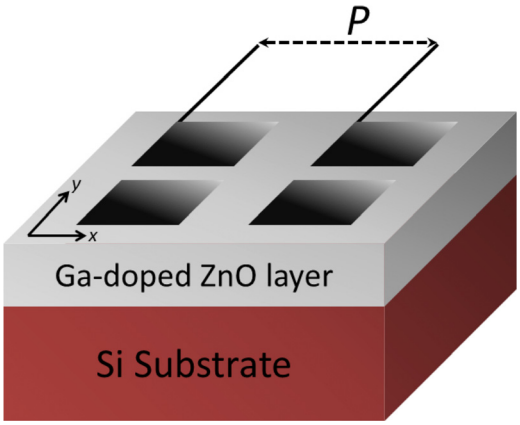

FIG. 1. Hole array structure of the device under investigation. Arrayed holes are etched into the Ga-doped ZnO layer.

$$k_{SPP} = \sqrt{\left(k_x + \frac{2\pi m}{P}\right)^2 + \left(\frac{2\pi n}{P}\right)^2} = 2\pi\sqrt{\left(\frac{n_d}{\lambda}\sin\theta + \frac{m}{P}\right)^2 + \left(\frac{n}{P}\right)^2}, \quad (2)$$

where P is assumed here to be uniform in each direction, λ is the incident wavelength which is the excitation wavelength for a specific mode, n_d is the index of the dielectric region where the SPP mode is excited, and m and n are positive and negative integers (0, ±1, ±2.) for forward and backward propagating SPP modes. It is worth noting that a SPP mode is forward (backward) propagating if its propagation direction lies along (opposite to) the in-plane component of the incident wavevector. In this work, the light will be TM polarized in the x-direction (Fig. 1). The incident light is at an angle θ between the x-axis and xy-surface normal with normally incident light being at $\theta = 0°$. Also for our structures, the intended SPP excitation occurs at the air and ZnO interface, leaving $\varepsilon_d = n_d = 1$.

Ga-doped ZnO layers were deposited on a silicon substrate via pulsed laser deposition (PLD).[14] The achieved layer was nominally $Zn_{0.974}Ga_{0.026}O$ with a doping level of $\sim 10^{21}\,cm^{-3}$ as measured by IR ellipsometry.[26] The layer thickness was measured to be $\sim 1.2\,\mu m$ with an uncertainty of ±71 nm using visible ellipsometry. The measured complex permittivities of the deposited layer along with the propagation length of SPP modes at the air/ZnO interface (L_x) are calculated[26] using the following equation and compared with those of the gold[34] in Fig. 2:

$$L_x = [2\,\mathrm{Im}(k_{spp})]^{-1}. \quad (3)$$

The real part of the Ga:ZnO permittivity crosses zero at 1.4 μm, which is denoted as λ_p, and becomes negative for $\lambda > \lambda_p$. In the wavelength range from 5 to 11 μm, the real part has values of −30 to −140 with the imaginary component taking positive values of 10–100 and the plasmon propagation length being 100–500 μm. These conditions are sufficient to support excitation of plasmonic modes at the interface with ZnO acting as the mid-IR range metal. The excited modes can then propagate along the interface for tens of periods (~6–10 μm), enabling an interaction with periodic structures that can result in evanescent out-coupling of the SPP modes through the subwavelength holes. In comparison, gold has permittivity, both real and imaginary, that is nearly 2 times larger in the regions of interest. These larger permittivity values leads to gold enabling much longer SPP propagation lengths than Ga:ZnO in the mid-IR. Gold, however, lacks SPP mode confinement, due to the operation wavelength being far from the bulk plasma wavelength, and CMOS compatibility, which makes it unsuitable for plasmonic applications in this infrared regime.

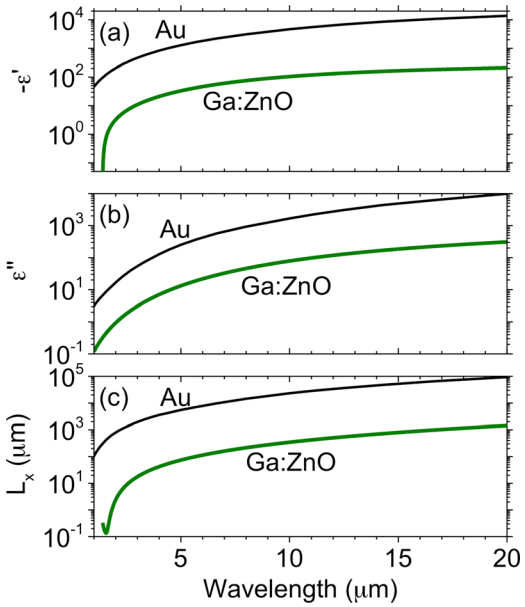

FIG. 2. (a) Real and (b) imaginary parts of the electric permittivity of the deposited $Zn_{0.974}Ga_{0.026}O$ layer with plasma wavelength of 1.4 μm and (c) propagation length of SPP modes at the air/ZnO interface. All data are compared with that of gold.

Square lattice arrays of circular and square holes with periods of 6, 8, and 10 μm and 50% duty cycle were transferred to the sample by a standard UV photolithography process. A 250 nm thick Ni film was then deposited on top and used as a metal hard mask after lift-off. The sample was then inductively coupled plasma (ICP) etched with BCl_3 using the recipe of Ref. 15. The etch process was run in multiple steps. The samples were first etched for 30 min after which the material compositions at the bottom of the holes were studied with energy dispersive x-ray spectroscopy (EDS) to find the Si and ZnO concentrations. The etch process was then continued at multiple shorter steps of 2.5 min for a total etch time of 37.5–40 min until low energy EDS confirmed high concentrations (above 90%) of Si indicating that the ZnO had mostly been etched through. The unknown thickness penetration for the electron beams in these materials leads to some ambiguity on the specific amount of ZnO left in the holes. Different etch times were due to slightly different ZnO thicknesses between samples.

Top-down and cross-section scanning electron microscope (SEM) images of a fabricated square-hole array sample with 10 μm period are shown in Figs. 3(a) and 3(b), respectively. The edges of the squares are slightly rounded,

which is expected for photolithography with the dimensions used. Fig. 3(b) confirms the completion of the etch process at the ZnO/Si interface as expected from EDS data, although in some of the samples the Si substrate was also etched due to varying ZnO layers thicknesses. The etched sidewalls are observed to be angled ~19° from vertical. SEM cross-section views of the fabricated structures revealed the presence of a thin rough ZnO film at the bottom of the holes, likely due to the deep micron sized etch profile. This was confirmed by high resolution SEM imaging of the bottom of a hole (Fig. 3(c)) and subsequent EDS analysis. When the x-ray beam is focused on a bright or dark area in Fig. 3(c), EDS returns a high content of ZnO or Si, respectively, confirming the presence of a rough ZnO film with varying thickness.

III. SIMULATIONS

In order to verify that plasmon resonance tunneling is indeed occurring, as opposed to the excitation of Fabry-Perot resonances or waveguide modes, E-field profiles from finite-difference time-domain (FDTD) simulations were analyzed on- and off-the ($m = 1$, $n = 0$) plasmon resonance. The simulations were performed using the commercially available Lumerical FDTD software. The wavelength-dependent complex permittivity values for Ga-doped ZnO layer, measured with spectroscopic IR ellipsometer and shown in Fig. 2, were imported into the software to use for the associated plasmonic layer. The Si substrate was defined by choosing Si as the substrate material in FDTD database, while the periodic etched hole arrays were simulated using the predefined "etched" material in the software database with the refractive index of 1. Symmetric and Bloch boundary conditions were chosen in *x*- and *y*-axis for simulations with normal and tilted incident angles, respectively. The boundary condition for *z*-axis was kept fixed as 12 perfect matching layers (PML) in both cases. The source was chosen to be a broadband plane wave with wavelength range of 2–15 μm incident top to down in reference to Fig. 1, along the *z*-axis and polarized along the *x*-axis.

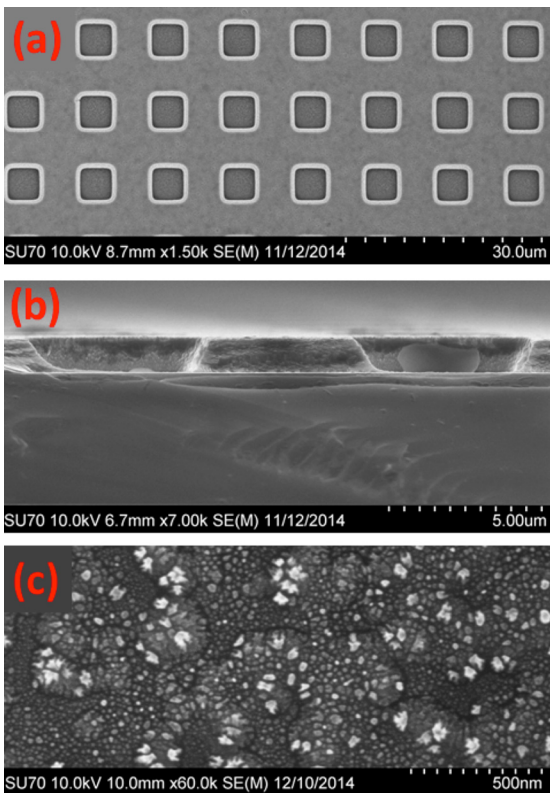

FIG. 3. (a) Top-down and (b) cross-section SEM images of a fabricated square-hole array with 10 μm period and 50% duty cycle along with (c) SEM image of the bottom of a hole.

Figures 4(a) and 4(b) show a side view of the E-field magnitude in logarithmic scale taken off- and on-the resonant wavelength for a device with 8 μm array period and 4 μm square hole size, respectively. In Fig. 4(b), the electric field is highly bound to the air/ZnO interface and concentrated at the surface edges of the hole arrays, consistent with the excitation of plasmons. As a result of the excited propagating SPP modes and their evanescent out-coupling to the periodic hole arrays, the transmitted E-field magnitude is increased by 2-orders of magnitude at the resonance wavelength.

Also presented in Fig. 4(c) is the simulated transmission spectrum of the periodic device along with the calculated diffraction limited baseline predicted by the theory of light transmission through subwavelength apertures. The transmission baseline is calculated for a 4 μm sized aperture in an opaque, black screen using the relations provided in Refs. 35 and 36. The diffraction limit predicts a transmission of ~10%–20% which decreases as a function of increasing wavelength. The periodic hole-array structure, however, shows strong transmission peaks as high as 65% at the wavelengths of plasmonic modes resonances, which is in agreement with the provided E-field mode profiles.

IV. EXPERIMENTAL RESULTS

Optical transmission and reflection spectra of the samples were measured with a Bruker Hyperion IR-microscope integrated with a Vertex 80v Fourier transform IR (FTIR) spectrometer. The microscope configuration was modified having objective and condenser lenses removed to have its broadband and TM-polarized IR beam collimated. This enabled us to measure the transmission and reflection spectra of the fabricated structure under normal incidence and avoid the broadening of resonance features due to a spread of illumination angles.

Figure 5 presents measured and simulated transmission and reflection spectra for the fabricated structures. Simulations were performed for the ideal etched structure. All spectra are for normally incident light in the wavelength range of 5–11 μm. Two resonance modes (m, $n = 1,0$ and 1,1) were observed as reflection dips along with their corresponding transmission peaks; however, only the strongest mode (1,0) is shown in Fig. 5 for clarity. All measured and simulated transmission spectra are normalized to account for the reflection at the Si/air interface and scaled to the opening percentage of the structures as determined by SEM. The spectra for 6, 8, and 10 μm period structures are shown with blue, green, and red curves, respectively. In both simulation and experiment, the (1, 0) SPP mode redshifts with increasing array period as predicted by Eq. (2). The observed transmission is slightly

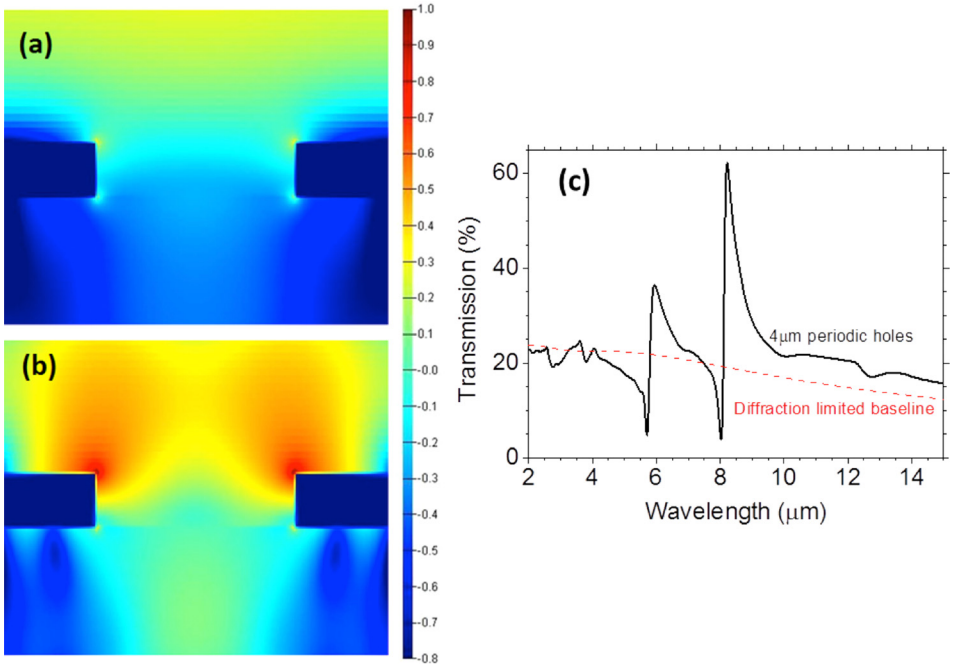

FIG. 4. FDTD simulated E-field profiles of the device with 8 μm array period and 4 μm square hole sizes (a) on-, and (b) off- (1, 0) plasmonic resonance. Also presented is the simulated transmission spectrum of the device along with the predicted diffraction limited baseline (c).

stronger for square hole arrays (solid lines) than for circular holes (dashed-dotted lines), which is indicative of stronger plasmonic coupling, as reported in Ref. 37 by Kuipers *et al*. It is also observed that the coupling efficiency increases with increasing array period. Simulation results predict ~250% for the relative transmission peaks for these structures. In the measured data, a maximum relative transmission of ~105% is achieved through sub-wavelength hole arrays in devices with 10 and 8 μm period square holes.

Further FDTD simulations were carried out to investigate a more accurate portrayal of the structures. The sidewall angle, the etch depth into the silicon substrate, and the presence of the thin rough ZnO film were determined from SEM cross-section images and utilized in the simulation. A truncated pyramid hole shape was used to simulate the structure observed in Fig. 3(b). Parameters utilized were array period of 8 μm, top opening of 4.26 μm, bottom opening of 3.06 μm, and etch depth of 1.74 μm (with ZnO thickness of 1.0 μm and etch depth of 0.74 μm into the Si). These structural changes resulted in slight, but not significant, decreasing of transmission.

In addition to these structural changes, we investigate the effects of the rough ZnO film. The determined maximum thickness of the film, ~100 nm, is an order of magnitude smaller than the overall deposited ZnO layer thickness (1.2 μm). This order of magnitude difference, allows this thin region to be treated as a thin film with a spatial average of ZnO and air permittivities, as described by the "effective

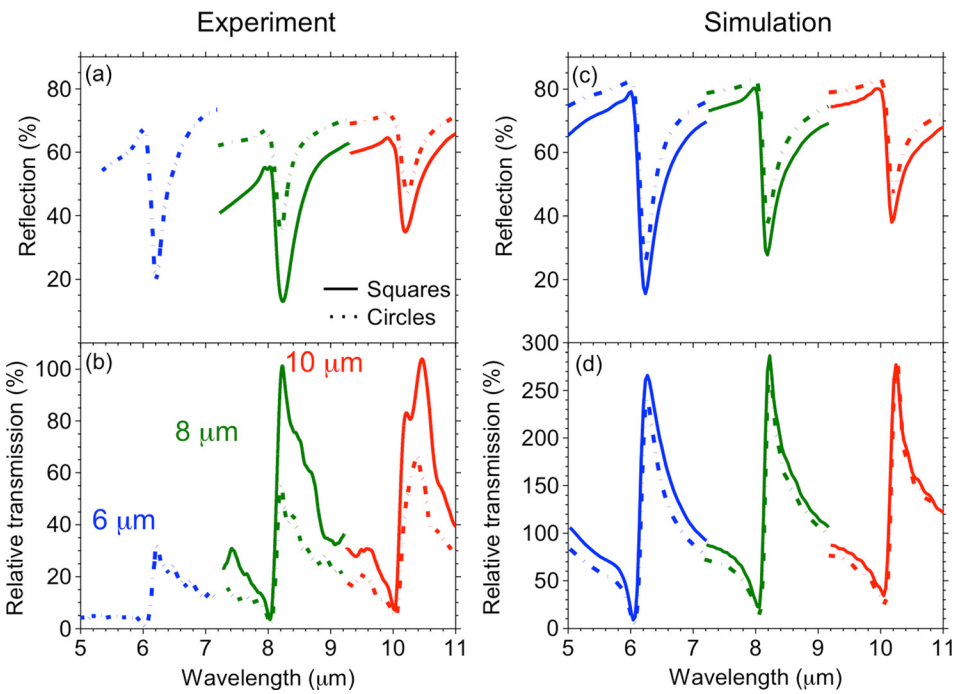

FIG. 5. Experimental and simulated reflection ((a) and (c)) and transmission ((b) and (d)) spectra of the fabricated structures for normally incident infrared light. Relative transmission spectra are the transmission through ZnO hole arrays normalized to that of Si substrate and scaled to the opening area.

medium approximation" or "50:50 model."[38–42] FDTD simulations were therefore completed with a 100 nm film in the hole using a 50/50 composition of the ZnO/air. The addition of this thin ZnO layer in the hole causes the relative transmission to decrease from 275% to 117%, which is within 10% of the measured data for 8 μm square holes. With the added rough ZnO film in the hole, the coupling of incident light to SPP's is actually increased which was observed as an intensification of the electric fields bound at the top ZnO/air interface and at the resonance wavelength. The stronger SPP mode still undergoes tunneling although the transmitted light is observed to decrease in both the electric field cross-section and transmission output which can be attributed to absorption in the thin rough layer. By using the above alterations from the ideal structure, piecewise simulations revealed the largest degradation in transmission strength, which was likely due to the rough ZnO film that remains in the holes, although the structure shape could have played a minimal role in the discrepancies between simulation and experiments.

Transmission spectra of the 8 μm period square hole arrays are shown in Fig. 6 for incident angles from 0° (top trace) to 18° (bottom trace) with average angular step size of 1.8°. To perform these measurements, the sample was mounted on a rotation stage and placed in the beam path. The sample was tilted about the optical axis of the microscope to obtain different incident angles. Data are presented for incident light with E-field polarized perpendicular to the axis of rotation. The transmission spectra show the decoupling of counter-propagating SPP modes as a function of increasing angle. At normal incidence, the counter propagating mode pairs of (±1, 0) and (±1, 1) are degenerate. Changing the angle of incidence from the surface normal red-shifts (blue-shifts) the forward (backward) propagating modes, removing the degeneracy. The observed shifting can be explained by the sign of the m-integer and the $\sin(\theta)$ factor in Eq. (2). Calculated locations of transmission maxima associated with the (1, 0), (−1, 0), (1, 1), and (−1, 1) SPP modes are determined using Eqs. (1) and (2) and presented in Fig. 6 as red triangles, blue triangles, red diamonds, and blue diamonds, respectively. Also plotted with dashed blue curves are FDTD simulated transmission spectra of the device for incident angles of 0° and 10.8°. The simulated curves are plotted next to their corresponding measured spectra for comparison. The simulated transmission peaks agree well with calculated SPP locations and experimental results. The measured transmission peaks at the (−1, 1) and (1, 1) resonances are, however, very weak again due to the presence of the thin rough ZnO film at the bottom of the holes.

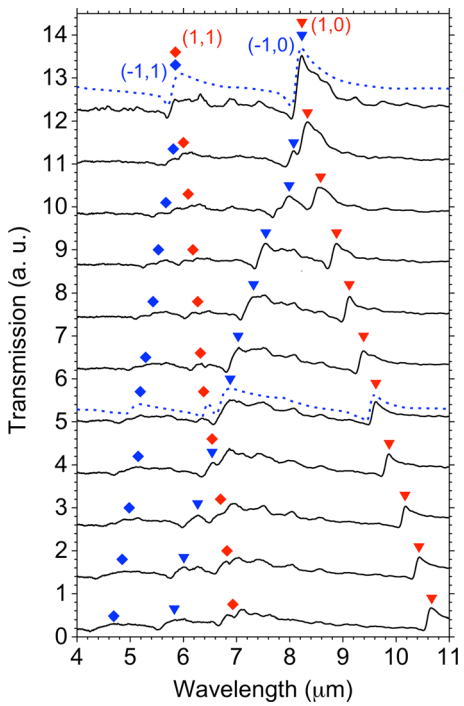

FIG. 6. Transmission spectra for 8 μm square hole arrays as a function of incident angle from 0° (top trace) to 18° (bottom trace) with angle step size of ~1.8°. Data are measured for incident light polarized perpendicular to the axis of rotation. Calculated values of excitation wavelengths for different SPP modes are also marked as scatter points with their mode numbers noted. Simulated transmission spectra at incident angles of 0° and 10.8° are also provided for comparison (dashed lines).

V. SUMMARY

In summary, we report the fabrication, simulation, and optical characterization of plasmon resonance enhanced IR optical transmission through square and circular hole arrays etched into a 1 μm thick Ga-doped ZnO layer on a silicon wafer. The samples were fabricated with 6, 8, and 10 μm array periods and 50% duty cycle. Simulations, along with optical measurements, reveal strong coupling of free space radiation to SPPs as observed by 40%–60% reflection dips in the IR spectra. Experimental results show array-period tunable resonant mode tunneling characteristics that are consistent with the plasmon excitation and evanescent out-coupling of such propagating SPP modes to periodic hole arrays, as evidenced by the agreement with simulated mode profiles and analytical calculations. Differences in transmission percentages between simulation and experiment can be explained by the presence of thin rough ZnO films at bottom of the etched holes and by imperfectly fabricated grating structures as confirmed by SEM cross-section images and EDS measurements. These experiments also show square holes in all cases out-performing circular holes in terms of SPP coupling and the consequent transmission features. Device transmission was also measured for angled incident light which removes the degeneracy for SPP modes that propagated oppositely while in the plane of the polarization. This degeneracy lifting agrees with analytical SPP theory and FDTD simulations. The results presented here provide a basis for a new class of plasmonic IR optical devices that are tailorable throughout the mid-infrared via both inherent doping and structural changes.

ACKNOWLEDGMENTS

N. Nader and J. W. Cleary acknowledge AFOSR LRIR No. 12RY10COR (Program Officer Dr. Gernot Pomrenke). J. R. Hendrickson would also like to acknowledge support by AFOSR under LRIR No. 12RY05COR (Program Officer Dr. Gernot Pomrenke). J. Guo acknowledges the support by

the National Science Foundation (NSF) through the Award No. NSF-1158862. D. C. Look acknowledges support by AFOSR Grant No. FA9550-10-1-0079 (K. Goretta) and NSF Award No. 1305193 (C. Ying).

[1]T. W. Ebbesen, H. J. Lezec, H. F. Ghaemi, T. Thio, and P. A. Wolff, Nature **391**, 667 (1998).
[2]C. Genet and T. W. Ebbesen, Nature **445**, 39 (2007).
[3]S. Law, V. Podolskiy, and D. Wasserman, Nanophotonics **2**, 103 (2013).
[4]H. Liu and P. Lalanne, Nature **452**, 728 (2008).
[5]J. V. Coe, J. M. Heer, S. Teeters-Kennedy, H. Tian, and K. R. Rodriguez, Annu. Rev. Phys. Chem. **59**, 179 (2008).
[6]E. Sachet, C. T. Shelton, J. S. Harris, B. E. Gaddy, D. L. Irving, S. Curtarolo, B. F. Donovan, P. E. Hopkins, P. A. Sharma, A. L. Sharma, J. Ihlefeld, S. Franzen, and J.-P. Maria, Nat. Mater. **14**, 414 (2015).
[7]T. Ribaudo, D. W. Peters, A. R. Ellis, P. S. Davids, and E. A. Shaner, Opt. Express **21**, 6837 (2013).
[8]S. Law, D. C. Adams, A. M. Taylor, and D. Wasserman, Opt. Express **20**, 12155 (2012).
[9]D. Wasserman, E. A. Shaner, and J. G. Cederberg, Appl. Phys. Lett. **90**, 191102 (2007).
[10]K. Anglin, T. Ribaudo, D. C. Adams, X. Qian, W. D. Goodhue, S. Dooley, E. A. Shaner, and D. Wasserman, J. Appl. Phys. **109**, 123103 (2011).
[11]B. S. Passmore, D. G. Allen, S. R. Vangala, W. D. Doohue, D. Wasserman, and E. A. Shaner, Opt. Express **17**, 10223 (2009).
[12]S. M. Williams, A. D. Stafford, T. M. Rogers, S. R. Bishop, and J. V. Coe, Appl. Phys. Lett. **85**, 1472 (2004).
[13]J. V. Coe, S. M. Williams, K. R. Rodriguez, S. Teeters-Kennedy, A. Sudnitsyn, and F. Hrovat, Anal. Chem. **78**, 1384 (2006).
[14]J. Zhao, X. Zhang, C. R. Yonzon, A. J. Haes, and R. P. Van Duyne, Nanomedicine **1**, 219–228 (2006).
[15]J. W. Cleary, N. Nader Esfahani, S. Vangala, J. Guo, J. R. Hendrickson, K. D. Leedy, and D. C. Look, Proc. SPIE **8987**, 898704 (2014).
[16]A. W. Murray and W. L. Barnes, Adv. Mater. **19**, 3771 (2007).
[17]P. R. West, S. Ishii, G. Naik, N. Emani, V. M. Shalaev, and A. Boltasseva, Laser Photonics Rev. **4**, 795 (2010).
[18]A. Boltasseva and H. A. Atwater, Science **331**, 290 (2011).
[19]G. Naik, J. Kim, and A. Boltasseva, Opt. Mater. Express **1**, 1090 (2011).
[20]R. Soref, R. E. Peale, and W. R. Buchwald, Opt. Express **16**, 6507 (2008).
[21]Y. Chen, Opt. Express **17**, 3130 (2009).
[22]J. W. Cleary, R. E. Peale, D. J. Shelton, G. D. Boreman, C. W. Smith, M. Ishigami, R. Soref, A. Drehman, and W. R. Buchwald, J. Opt. Soc. Am. B **27**, 730 (2010).
[23]J. C. Ginn, R. L. Jarecki, Jr., E. A. Shaner, and R. S. Davids, J. Appl. Phys. **110**, 043110 (2011).
[24]M. Shahzad, G. Medhi, R. E. Peale, W. R. Buchwald, J. W. Cleary, R. Soref, G. D. Boreman, and O. Edwards, J. Appl. Phys. **110**, 123105 (2011).
[25]J. W. Cleary, G. Medhi, M. Shahzad, I. Rezadad, D. Maukonen, R. E. Peale, G. D. Boreman, S. Wentzell, and W. R. Buchwald, Opt. Express **20**, 2693 (2012).
[26]J. W. Cleary, M. R. Snure, K. D. Leedy, D. C. Look, K. Eyink, and A. Tiwari, Proc. SPIE **8545**, 854504 (2012).
[27]M. Snure and A. Tiwari, J. Appl. Phys. **101**, 124912 (2007).
[28]S. Pearton, M. Snure, D. Toledo, P. Slusser, and A. Tiwari, *GaN and ZnO-Based Materials and Devices* (Springer-Verlag, Berlin, Heidelberg, 2012), p. 349.
[29]D. C. Look and K. D. Leedy, Proc. SPIE **8263**, 826302 (2012).
[30]M. Allen, J. W. Allen, B. R. Wenner, D. C. Look, and K. D. Leedy, Proc. SPIE **8626**, 862605 (2013).
[31]M. Allen, J. W. Allen, B. R. Wenner, D. C. Look, and K. D. Leedy, Opt. Eng. **52**, 064603 (2013).
[32]J. W. Cleary, N. Nader Esfahani, S. Vangala, J. Guo, J. R. Hendrickson, K. D. Leedy, D. Thomson, and D. C. Look, Proc. SPIE **8809**, 88090L (2013).
[33]H. Raether, *Surface Plasmons on Smooth and Rough Surfaces and on Gratings* (Springer, New York, 1988).
[34]M. A. Ordal, R. J. Bell, R. W. Alexander, Jr., L. L. Long, and M. R. Querry, Appl. Opt. **26**, 744 (1987).
[35]J. Weiner, Rep. Prog. Phys. **72**, 064401 (2009).
[36]M. K. Kowarz, Appl. Opt. **34**(17), 3055 (1995).
[37]K. J. K. Koerkamp, S. Enoch, F. B. Cegerink, N. F. van Hulst, and L. Kuipers, Phys. Rev. Lett. **92**, 183901 (2004).
[38]D. Lehmann, F. Seidel, and D. R. T. Zahn, SpringerPlus **3**, 82 (2014).
[39]O. D. Gordan, T. Sakurai, M. Friedrich, K. Akimoto, and D. R. T. Zahn, Org. Electron. **7**, 521 (2006).
[40]O. D. Gordan, S. Hermann, M. Friedrich, and D. R. T. Zahn, J. Phys. IV Fr. **132**, 73 (2006).
[41]J. Sindu Louis, D. Lehmann, M. Fredrich, and D. R. T. Zahn, J. Appl. Phys. **101**, 013503 (2007).
[42]I. Volintiru, M. Creatore, and M. C. M. van de Sanden, J. Appl. Phys. **103**, 033704 (2008).